Supporting Information

Liquid Crystalline Self-Assembly of Azulene-Thiophene Hybrids and their Applications as OFET Materials

Finn Schulz,[a,b] Shun Takamaru[b], Tobias Bens[c], Jun-ichi Hanna[b], Biprajit Sarkar*[,c], Sabine Laschat*[,a] and Hiroaki Iino*[,b]

[a] *Institut für Organische Chemie, Universität Stuttgart, Pfaffenwaldring 55, D-70569 Stuttgart, Germany*

[b] *Imaging Science and Engineering Research Center, Tokyo Institute of Technology, J1-2, 4259 Nagatsuta, Midori-ku, Yokohama 226-8503, Japan*

[c] *Institut für Anorganische Chemie, Universität Stuttgart, Pfaffenwaldring 55, D-70569 Stuttgart, Germany*

Contact:

Sabine Laschat; sabine.laschat@oc.uni-stuttgart.de.

Hiroaki Iino; iino@isl.titech.ac.jp.

Biprajit Sarkar; sarkar@iac.uni-stuttgart.de

Table of Contents

1. Methods

General methods: 2-Bromo-6-dodecyloxyazulene[1] **12O-Az-Br** and 2-(benzo[b]thiophen-2-yl)-4,4,5,5-tetramethyl-1,3,2-dioxaborolane[2] were synthesized according to the literature. All chemicals were, unless otherwise stated, used without further purification. The eluents for chromatography (hexanes, low boiling, and ethyl acetate EtOAc) were distilled prior to use. ^{1}H NMR spectra were measured using the Bruker Avance 500, and Bruker Avance 700 spectrometers at 500 MHz, and 700 MHz as well as ^{13}C NMR spectra at 126 MHz, and 176 MHz, respectively. To assign the signals of the ^{1}H and ^{13}C NMR spectra, COSY, HSQC, and HMBC measurements were carried out. FT-IR spectra were measured on a Bruker Vektor 22 with a MKII Golden Gate Single Reflection Diamond ATR. Absorption bands were rounded to integer wavenumbers / cm^{-1} and the absorption intensities were classified as follows: w (weak), m (medium), s (strong). Mass spectra (MS) and high-resolution mass spectra (HRMS) were measured by electrospray ionization (ESI) or electron impact ionization (EI) with a Bruker MicrOTOF-Q spectrometer or electron impact ionization (EI) with a *Varian MAT 711* spectrometer. For thin layer chromatography, silica gel 60 F254 glass plates (layer thickness of 0.25 mm) on aluminium (pore size 60 Å) from Merck were used. Column chromatography was performed using silica gel (particle diameter of 40 – 60 µm) from Fluka.

Polarizing Optical Microscopy: A polarizing optical microscope Olympus BX 50, equipped with a Linkam LTS heating stage, was used. Temperature regulation was carried out with the control units TP93 and LNP from Linkam ($\Delta T = \pm 1$ K). Photographs were saved with a digital camera ColorView from Soft Imaging System using the software analySIS.

Differential Scanning Calorimetry: For differential scanning calorimetry, a DSC822e from the company Mettler Toledo was employed. The compounds were analyzed in 40 µL sealed aluminum pans. Heating and cooling rates of 5 K min^{-1} were employed. Phase transition temperatures and enthalpies were determined by onset values using the software STARe 7.01.

SAXS and WAXS measurements: Measurements of the X-ray diffraction in the liquid crystalline phase were performed using a Bruker AXS Nanostar C with a ceramic tube generator (1500 W) having cross-coupled Goebel mirrors providing monochromatic Cu Kα radiation (1.5405 Å). Diffraction patterns were recorded with Bruker HI-STAR or VÅNTEC 500 detectors. Calibration was carried out using the diffraction pattern of silver behenate at

room temperature. The compounds were examined in sealed glass capillaries from Hilgenberg GmbH (external diameter of 0.7 mm, wall thickness 0.01 mm). Measured values were analyzed with the software SAXS from Bruker. The diffraction patterns were further processed using the software Datasqueeze and Origin. Fits were obtained using origin software and the goodness of fit judged by the reduced χ^2 value and residual plot shape. For the assignment of the Miller indices. The program LCDiXRay was used.[3]

Electrochemistry: Cyclic voltammograms were recorded with a PalmSens4 potentiostat with a conventional three-electrode configuration consisting of a frehsly polished (0.05 μm polishing alumin) platinum working electrode ($\varnothing$ = 2 mm, CH Instruments Inc.), a platinum auxiliary electrode, and a coiled silver wire as a pseudoreference electrode. The decamethylferrocene/decamethylferrocenium couple was used as internal reference. All measurements were performed at room temperature with a scan rate between 25 and 1000 mVs^{-1}. The experiments were carried out in dried and freshly destilled (CaH_2) CH_2Cl_2 containing 0.1 M Bu_4NPF_6 (Sigma-Aldrich, $\geq$ 99.0%, electrochemical grade) as the supporting electrolyte. The electrolyte was heated in the electrochemical cell under high vakuum to remove remaining crystal water.

Thin film fabrication and characterization: Thin films were fabricated on heavily p-doped silicon substrates with a 300 nm thick thermally grown silicon dioxide layer as the gate electrode and insulator. We used a 0.5 wt% p-xylene solution of **12O-Az-Ar** at 120 °C, and polycrystalline thin films were fabricated by spin-coating on the substrate at 60 °C [which is in the range of a highly ordered liquid crystal phase of smectic E (SmE)] at 3000 rpm or 1500 rpm for 30 s. Au with thickness of 30 nm was vacuum-evaporated at 3×10^{-4} Pa to form source/drain electrodes using a shadow mask. The channel length (L)/width (W) were 100/500 μm for normal measurements. For the transfer length method, the W/L ratio was 5 with L= 20; 30; 50; 100; 150 μm.

The resulting films were evaluated by optical microscopy, confocal laser scanning microscopy (VK-9700, Keyence), and atomic force microscopy (AFM, SPA300 DFM in tapping mode, Seiko) and in-plane and out-of-plane XRD (Smart Lab, Rigaku).

FET measurements:

The FET performance was characterized by two source measurement units (8252, ADCMT). The mobility (μ) was calculated by plotting the square root of the source-drain current (I_{ds}) versus gate voltage (V_g) and using the equation from the saturated region,

$$I_d = \frac{\mu W C_i}{2L}\left(V_g - V_{th}\right)^2$$

where C_i is capacitance of gate insulator and V_{th} is threshold voltage. One substrate, ~1.5 × 1.5 mm has 10 FET devices.

For calculation of the contact resistance via TLM following equations were used:

$$R_{total} \cdot W = \frac{L}{\mu C_i\left(V_g - V_{th}\right)} + R_{contact} \cdot W$$

$$R_{total} \cdot W = \frac{V_{ds}}{I_{ds}} \cdot W$$

Quantum chemical calculations: We employed DFT calculations using the B3LYP functional[4] with the multipole accelerated Resolution of the Identity approximation [5–7], dispersion correction[8] and BJ-damping[9]. A def2-TZVP basis set and appropriate auxiliary basis sets[10,11] were used. For numerical integrations m3 grid size was used. Structure optimizations with ethyl chains instead of dodecyl chains were carried out at this level of theory. The TURBOMOLE program package (Version 6.4)[12,13] was used throughout.

2. Synthesis and Characterization

General Procedure for the Synthesis of 6-Dodecyloxy-2-arylazulene at the example of 2-(6-Dodecyloxyazulene-2-yl)thiophene (GP1)

2-Bromo-6-dodecyloxyazulene (1.20 g, 3.07 mmol), thiophene-2 boronic acid (785 mg, 6.13 mmol) and Cs_2CO_3 (2.00 g, 6.13 mmol) were dissolved in dioxane (50 mL). The mixture was degassed for 30 min, then $Pd(PPh_3)_4$ (177 mg, 0.15 mmol) was added, and the reaction was refluxed for 3 h. After cooling down, silica gel was added, and the solvent was removed under reduced pressured. Purification was performed by column chromatography on silica gel with an adequate solvent mixture and subsequent recrystallizations.

2-(6-Dodecyloxyazulene-2-yl)thiophene 12O-Az-T

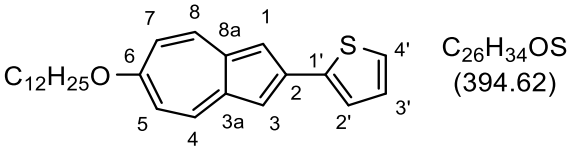

$C_{26}H_{34}OS$
(394.62)

Synthesis according to GP1; Reagents: 2-bromo-6-dodecyloxyazulene (1.20 g, 3.07 mmol), thiophene-2 boronic acid (785 mg, 6.13 mmol), Cs_2CO_3 (2.00 g, 6.13 mmol), $Pd(PPh_3)_4$ (177 mg, 0.15 mmol), dioxane (50 mL); Purification: Flash column chromatography on silica gel (Gradient: hexanes→ dichloromethane) (brown spot) and subsequent recrystallization from isopropylic alcohol. Yield: 70 %, brown solid (850 mg, 2.15 mmol)

Melting behavior: Cr 96 °C SmE 186 °C I (DSC, 1st heating); ^{1}H-NMR (700 MHz, $CDCl_3$): δ = 0.89 (t, J = 7.0 Hz, 3H, CH_3), 1.23–1.40 (m, 16H, CH_2), 1.46–1.52 (m, 2H, $OCH_2CH_2CH_2$), 1.81–1.87 (m, 2H, OCH_2CH_2), 4.08 (t, J = 6.5 Hz, 2H, OCH_2), 6.77–6.81 (m, 2H, 5-H, 7-H), 7.10 (dd, J = 5.0 Hz, 3.6 Hz, 1H, 3'-H), 7.29 (dd, J = 5.0 Hz, 1.0 Hz, 1H, 4'-H), 7.42 (s, 2H, 1-H, 3-H), 7.48 (dd, J = 3.6 Hz, 1.0 Hz, 1H, 2'-H), 8.05–8.09 (m, 2H, 4-H, 8-H) ppm; ^{13}C-NMR (176 MHz, $CDCl_3$): δ = 14.2, 22.7, 26.1, 29.3, 29.4, 29.6, 29.6, 29.7, 29.7, 32.0, 68.9, 112.0, 114.9, 124.3, 125.2, 128.2, 135.1, 136.9, 139.1, 141.5, 166.2 ppm;. FT-IR (ATR): $\tilde{\nu}$ = 2954 (w), 2917 (s), 2849 (s), 1585 (m), 1543 (w), 1464 (m), 1414 (w), 1382 (w), 1310 (w), 1294 (w), 1251 (w), 1235 (m), 1191 (s), 1159 (w), 1115 (w), 1000 (w), 906 (w), 837 (m), 823 (m), 803 (w), 728 (w), 681 (m), 649 (w), 494 (w), 425 (w) cm^{-1}; MS (EI): *m/z* for $C_{26}H_{34}OS^+$ calc.: 394.2 $[M]^+$, found.: 394.3; HRMS (EI): *m/z* for $C_{26}H_{34}OS^+$ calc.: 394.2330 $[M]^+$, found.: 394.2330.

3-(6-Dodecyloxyazulene-2-yl)thiophene 12O-Az-iT

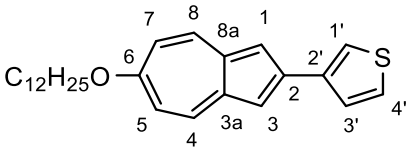

$C_{26}H_{34}OS$
(394.62)

Synthesis according to GP1; Reagents: 2-bromo-6-dodecyloxyazulene (141 mg, 360 µmol), thiophene-3 boronic acid (92 mg, 720 µmol), Cs_2CO_3 (235 mg, 721 µmol), $Pd(PPh_3)_4$ (21 mg, 18 µmol), dioxane (10 mL); Purification: Flash column chromatography on silica gel (toluene) and subsequent recrystallization from an isopropylic alcohol / chloroform mixture (20/1). Yield: 78 %, violet solid (113 mg, 286 µmol)

Melting behavior: Cr 107 °C SmE 229 °C I (DSC, 1st heating); ^{1}H-NMR (700 MHz, $CDCl_3$): δ = 0.88 (t, J = 7.0 Hz, 3H, CH_3), 1.23–1.40 (m, 16H, CH_2), 1.46–1.52 (m, 2H, $OCH_2CH_2CH_2$), 1.82–1.88 (m, 2H, OCH_2CH_2), 4.08 (t, J = 6.5 Hz, 2H, OCH_2), 6.77–6.82 (m, 2H, 5-H, 7-H), 7.38 (dd, J = 4.9 Hz, 2.9 Hz, 1H, 3'-H), 7.44 (s, 2H, 1-H, 3-H), 7.58 (dd, J = 5.0 Hz, 1.3 Hz, 1H, 4'-H), 7.66 (dd, J = 2.8 Hz, 1.3 Hz, 1H, 1'-H), 8.09–8.12 (m, 2H, 4-H, 8-H) ppm; ^{13}C-NMR (176 MHz, $CDCl_3$): δ = 14.1, 22.7, 26.1, 29.3, 29.4, 29.4, 29.6, 29.6, 29.7, 29.7, 31.9, 68.9, 111.7, 115.4, 121.1, 125.9, 127.0, 135.1, 136.9, 139.2, 140.6, 166.2 ppm; FT-IR (ATR): $\tilde{\nu}$ = 2954 (w), 2916 (s), 2871 (m), 2848 (s), 1582 (m), 1545 (m), 1471 (m), 1418 (m), 1390 (w), 1341 (w), 1294 (w), 1250 (m), 1229 (m), 1189 (s), 1158 (m), 1088 (w), 108 (w), 1000 (w), 874 (w), 840 (s), 829 (m), 816 (w), 782 (s), 773 (s), 756 (w), 728 (w), 689 (w), 599 (m) cm^{-1}; MS (EI): *m/z* for $C_{26}H_{34}OS^+$ calc.: 394.2 $[M]^+$, found.: 394.2; HRMS (EI): *m/z* for $C_{26}H_{34}OS^+$ calc.: 394.2330 $[M]^+$, found.: 394.2329.

2-(6-(dodecyloxy)azulen-2-yl)benzo[b]thiophene 12O-Az-BT

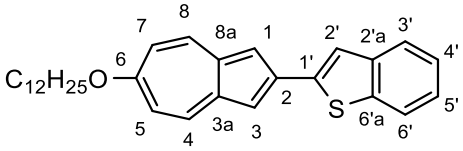

$C_{30}H_{36}OS$
(444.68)

Synthesis according to GP1; Reagents: 2-Bromo-6-Dodecyloxyazulene (99 mg, 253 µmol), 2-(benzo[b]thiophen-2-yl)-4,4,5,5-tetramethyl-1,3,2-dioxaborolane (99 mg, 379 µmol), Cs_2CO_3 (165 mg, 506 µmol), $Pd(PPh_3)_4$ (15 mg, 13 µmol), Dioxane (10 mL); Purification: Flash column chromatography on silica gel (Gradient: hexanes / ethyl acetate 10 / 1 → $CHCl_3$) (front line in $CHCl_3$) and subsequent recrystallization from ethyl acetate / chloroform (5 / 1). Yield: 72 %, brown solid (81 mg, 182 µmol)

Melting behavior: Cr 98 °C SmE 270 °C I (DSC, 1st heating); ^{1}H-NMR (700 MHz, toluene-d8, 80°C): δ = 0.92 (t, J = 7.1 Hz, 3H, CH_3), 1.26–1.45 (m, 18H, CH_2), 1.63–1.70 (m, 2H, OCH_2CH_2), 3.73 (t, J = 6.4 Hz, 3H, OCH_2), 6.61 (d, J = 10.8 Hz, 2H, 5-H, 7-H), 7.05–7.08 (m, 1H, 4'-H/5'-H), 7.15–7.18 (m, 1H, 4'-H/5'-H), 7.49 (s, 2H, 1-H, 3-H), 7.53 (s, 1H, 2'-H), 7.57–7.61 (m, 2H, 3'-H, 6'-H), 7.82–7.88 (m, 2H, 4-H, 8-H) ppm; ^{13}C-NMR (176 MHz, toluene-d6, 80°C): δ = 14.1, 23.0, 26.4, 29.7, 29.7, 29.7, 30.0, 30.0, 30.1, 30.1, 32.3, 69.1, 112.3, 116.7, 121.0, 122.5, 123.8, 124.4, 124.6, 135.7, 139.9, 140.8, 141.7, 142.0, 166.9 ppm; MS (EI): *m/z* for $C_{30}H_{36}OS^+$ calc.: 444.2 $[M]^+$, found.: 444.2; HRMS (EI): *m/z* for $C_{30}H_{36}OS^+$ calc.: 444.2481 $[M]^+$, found.: 444.2495. FT-IR (ATR): $\tilde{\nu}$ = 2955 (w), 2916 (s), 2849 (m), 1584 (m), 1543 (w), 1472 (w), 1416 (w), 1245 (w), 1192 (m), 1020 (w), 838 (m), 823 (s), 740 (m), 725 (m), 562 (w), 513 (w) cm^{-1}.

3. Differential Scanning Calorimetry

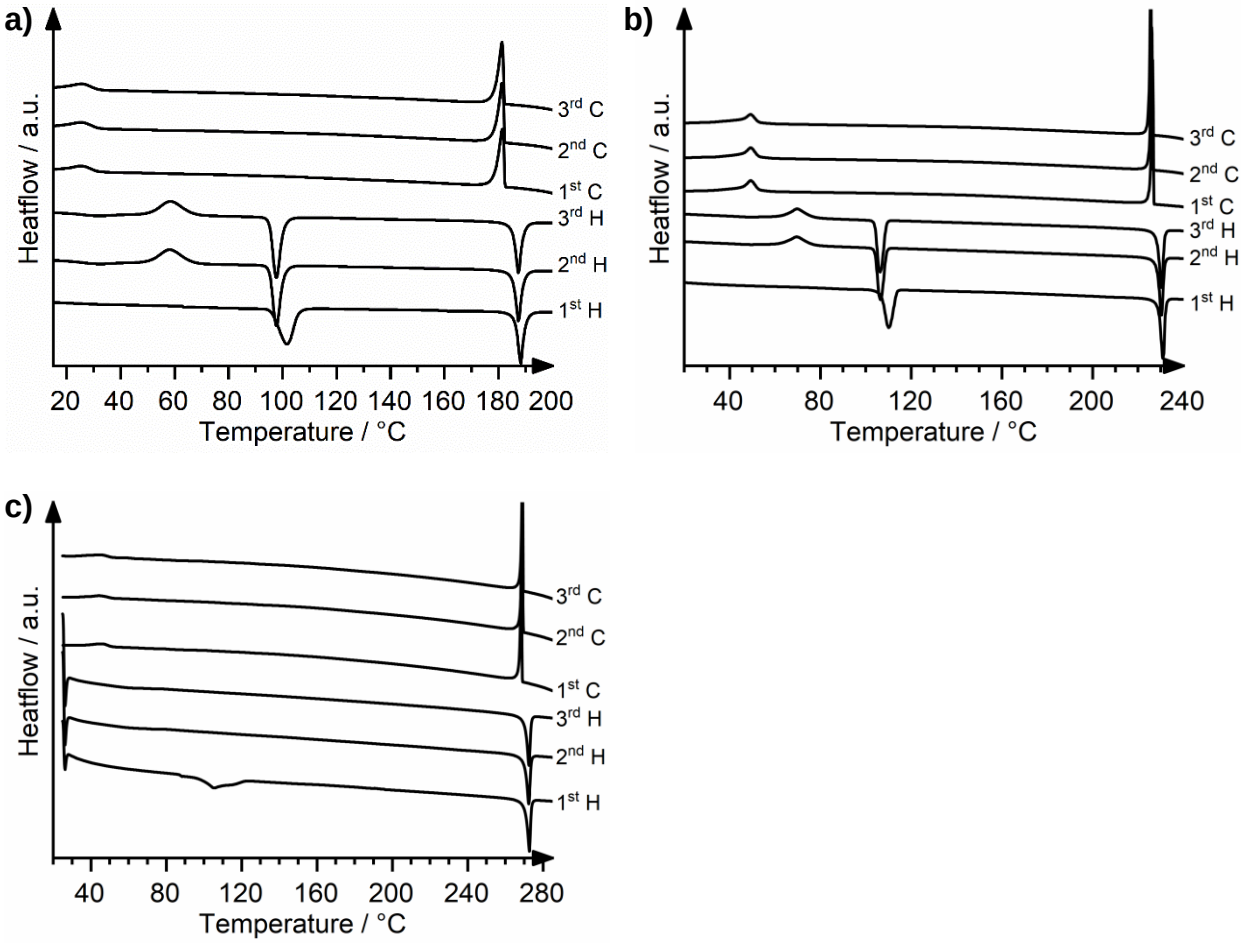

Figure S1: DSC-curves of the synthesized compounds: a) **12O-Az-T**, b) **12O-Az-iT** and c) **12O-Az-BT**. Heating/Cooling rate: 5 K/min.

4. Polarized Optical Microscopy

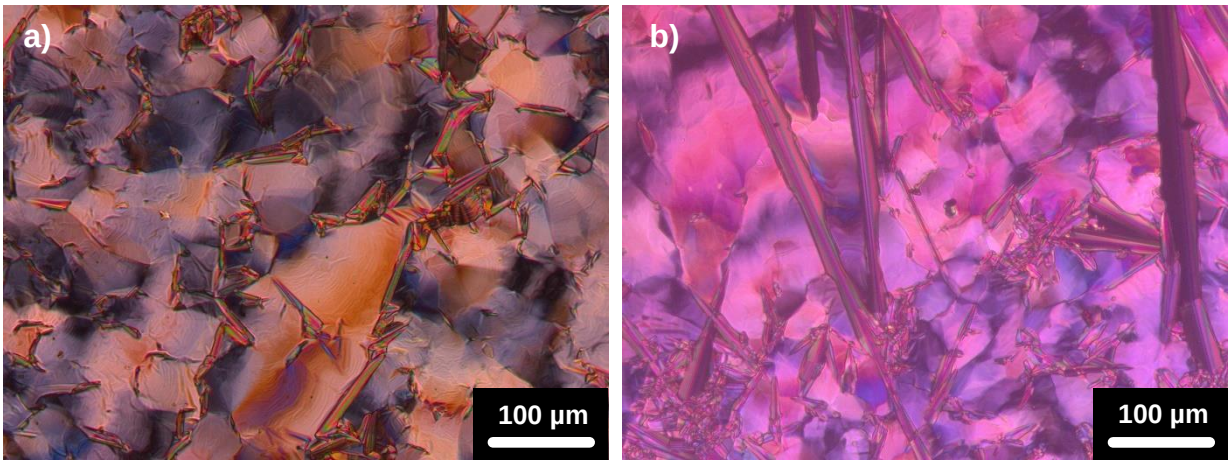

Figure S2: Platelet textures of a) **12O-Az-BT** at 268 °C and b) **12O-Az-T** at 188 °C between crossed polarizers.

5. X-Ray Diffractometry

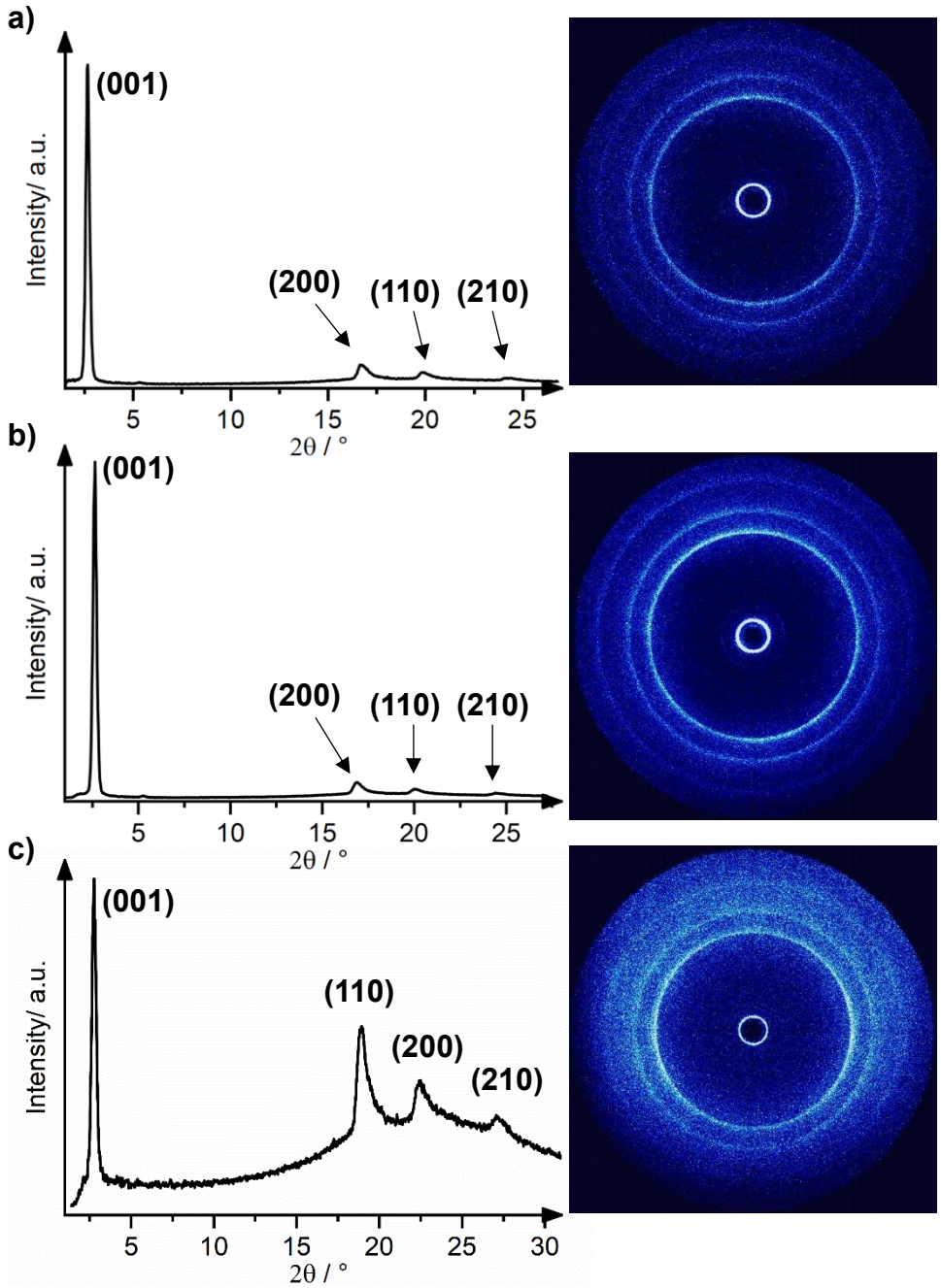

Figure S3: WAXS diffractogram and the corresponding diffraction pattern in the SmE phase of a) **12O-Az-T** at 115 °C, b) **12O-Az-iT** at 118 °C and c) **12O-Az-BT** at 143 °C.

6. Electrochemistry

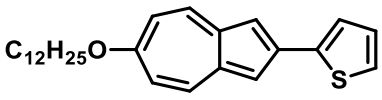

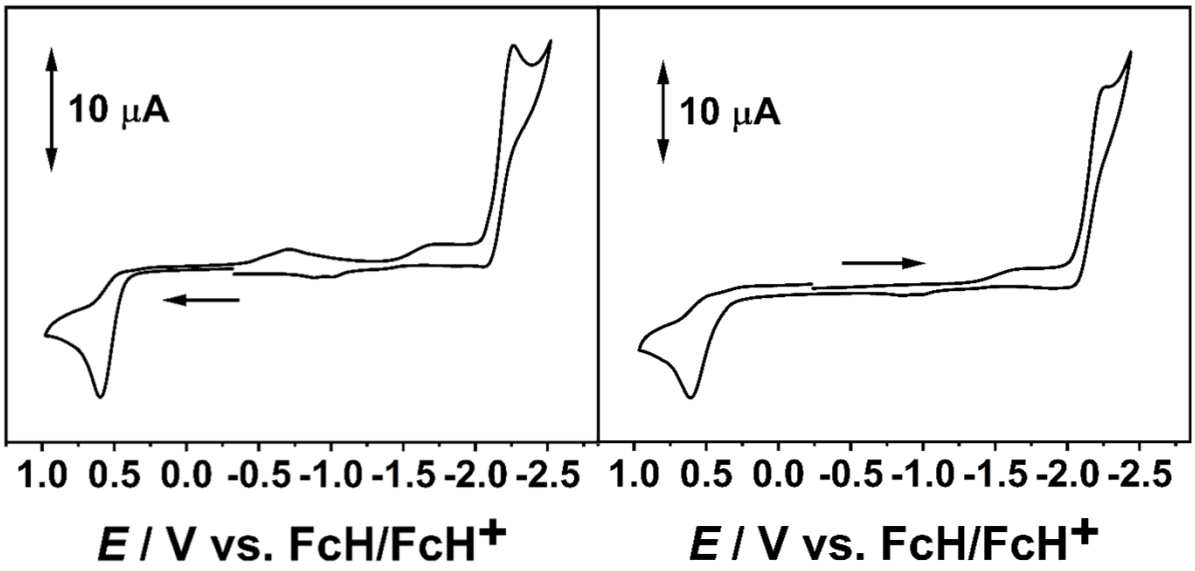

Figure S4: Cyclic voltammogram of sample **12O-Az-T** in CH_2Cl_2 and 0.1 M NBu_4PF_6 at scan rate of 100 mV/s with a Pt working electrode (left: oxidation first, right: reduction first).

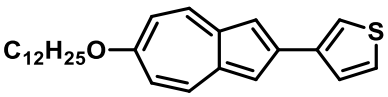

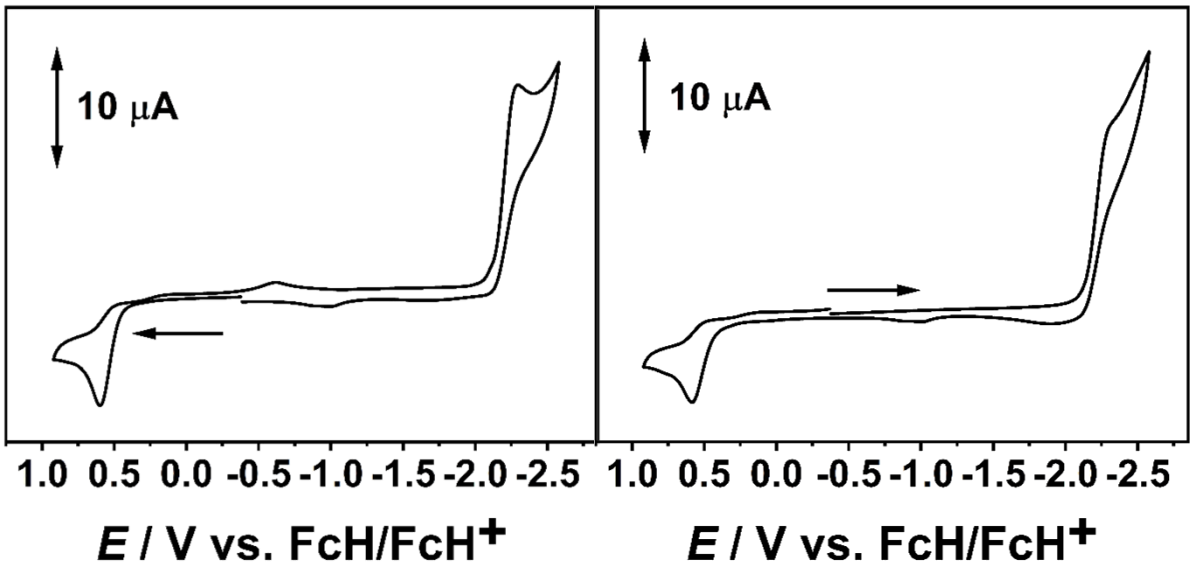

Figure S5: Cyclic voltammogram of sample **12O-Az-iT** in CH_2Cl_2 and 0.1 M NBu_4PF_6 at scan rate of 100 mV/s with a Pt working electrode (left: oxidation first, right: reduction first).

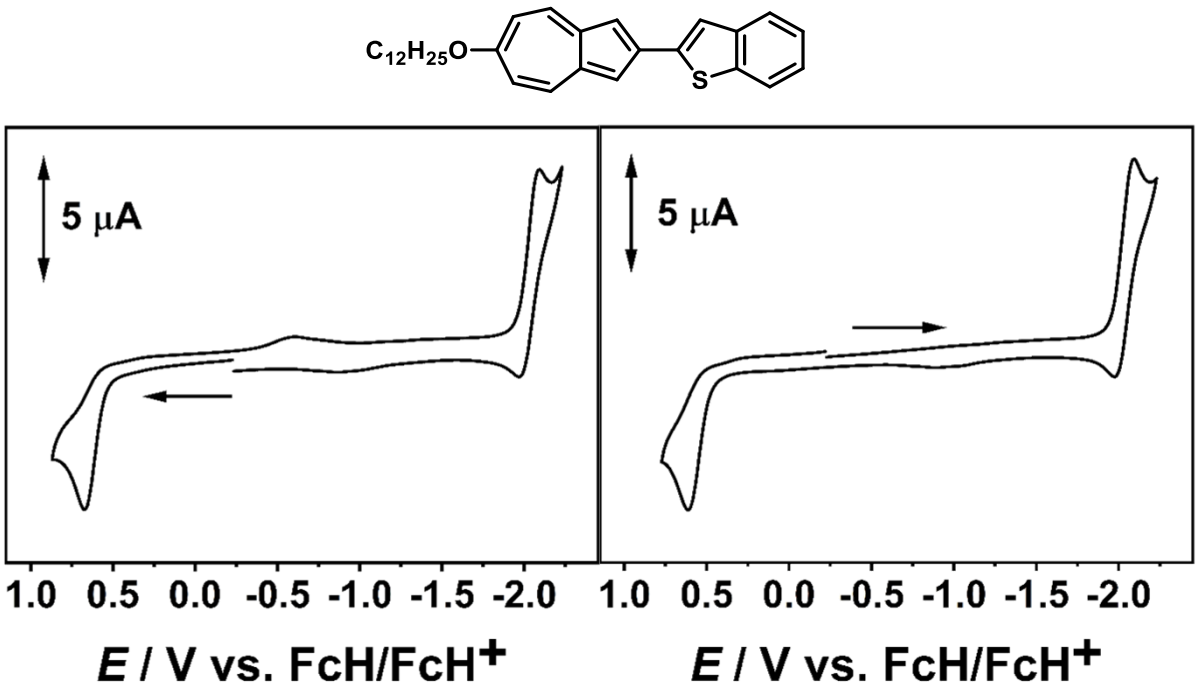

Figure S6: Cyclic voltammogram of sample **12O-Az-BT** in CH_2Cl_2 and 0.1 M NBu_4PF_6 at scan rate of 100 mV/s with a Pt working electrode (left: oxidation first, right: reduction first)

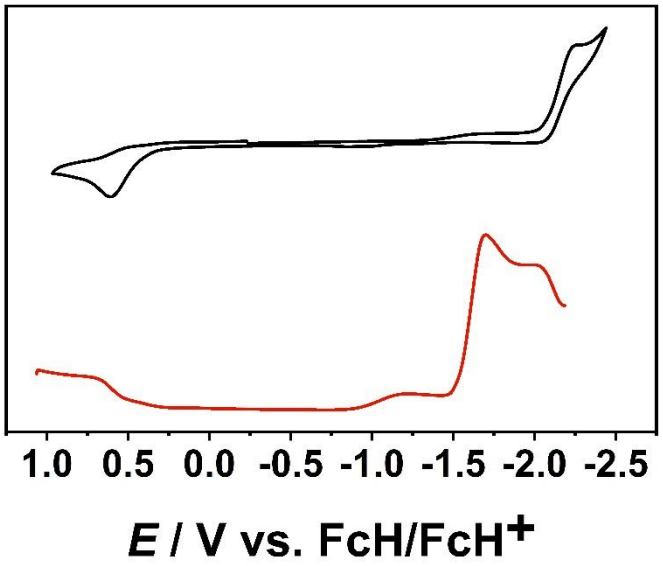

Figure S7: Differential pulse voltammetry of sample **12O-Az-T** in CH_2Cl_2 and 0.1 M NBu_4PF_6.

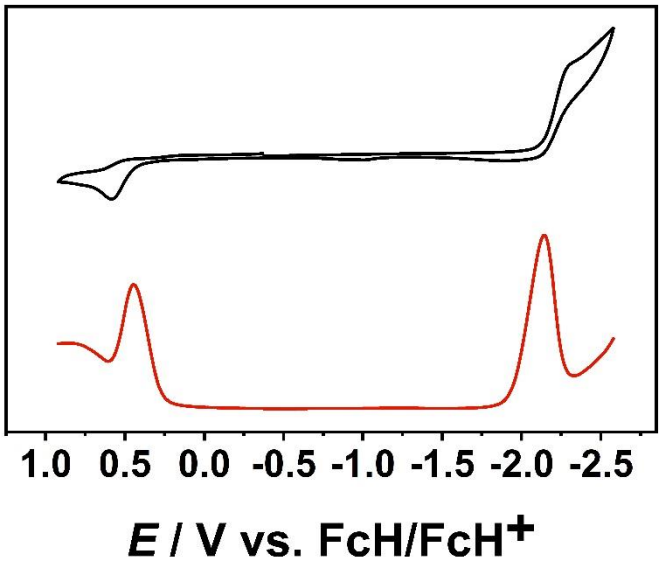

Figure S8: Differential pulse voltammetry of sample **12O-Az-iT** in CH_2Cl_2 and 0.1 M NBu_4PF_6.

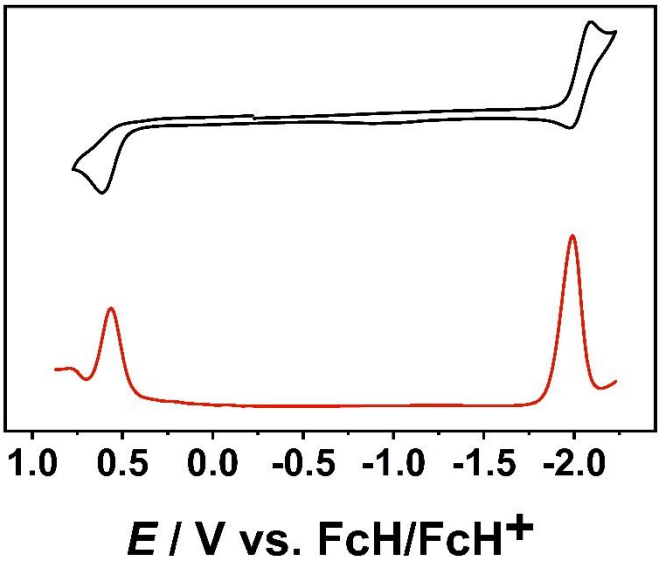

Figure S9: Differential pulse voltammetry of sample **12O-Az-BT** in CH_2Cl_2 and 0.1 M NBu_4PF_6.

Table S1: Electrochemical data of **12O-Az-Ar**.

Compound	$E_{pa,ox}$ / V	Oxidation	$E_{pc,red}$ / V	Reduction
12O-Az-T	+0.59	irreversible	−2.27	irreversible
12O-Az-iT	+0.60	irreversible	−2.29	irreversible
12O-Az-BT	+0.67	irreversible	−2.09	quasi-reversible

7. Optical Microscopy and Confocal Laser Scanning Microscopy

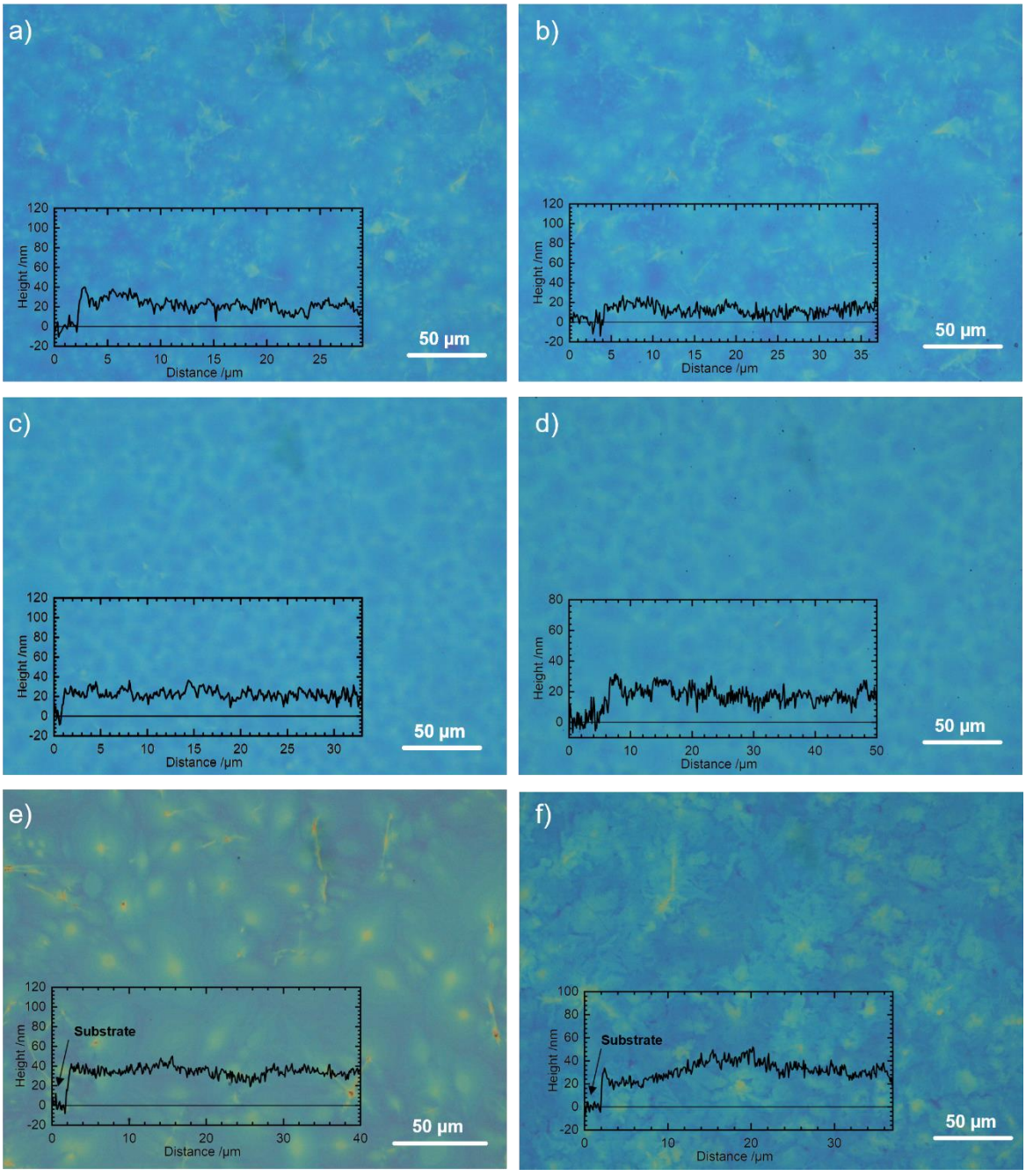

Figure S10: Optical microscopy images of polycrystalline thin films fabricated by spin-coating a 0.5 wt-% solution in *p*-xylene at 60 °C. Insets show cross-sectional profiles observed by confocal laser scanning microscopy: a),b) **12O-Az-iT** as coated and annealed, c),d) **12O-Az-T** as coated and annealed and e,f) **12O-Az-BT** as coated an annealed

8. Atomic Force Microscopy

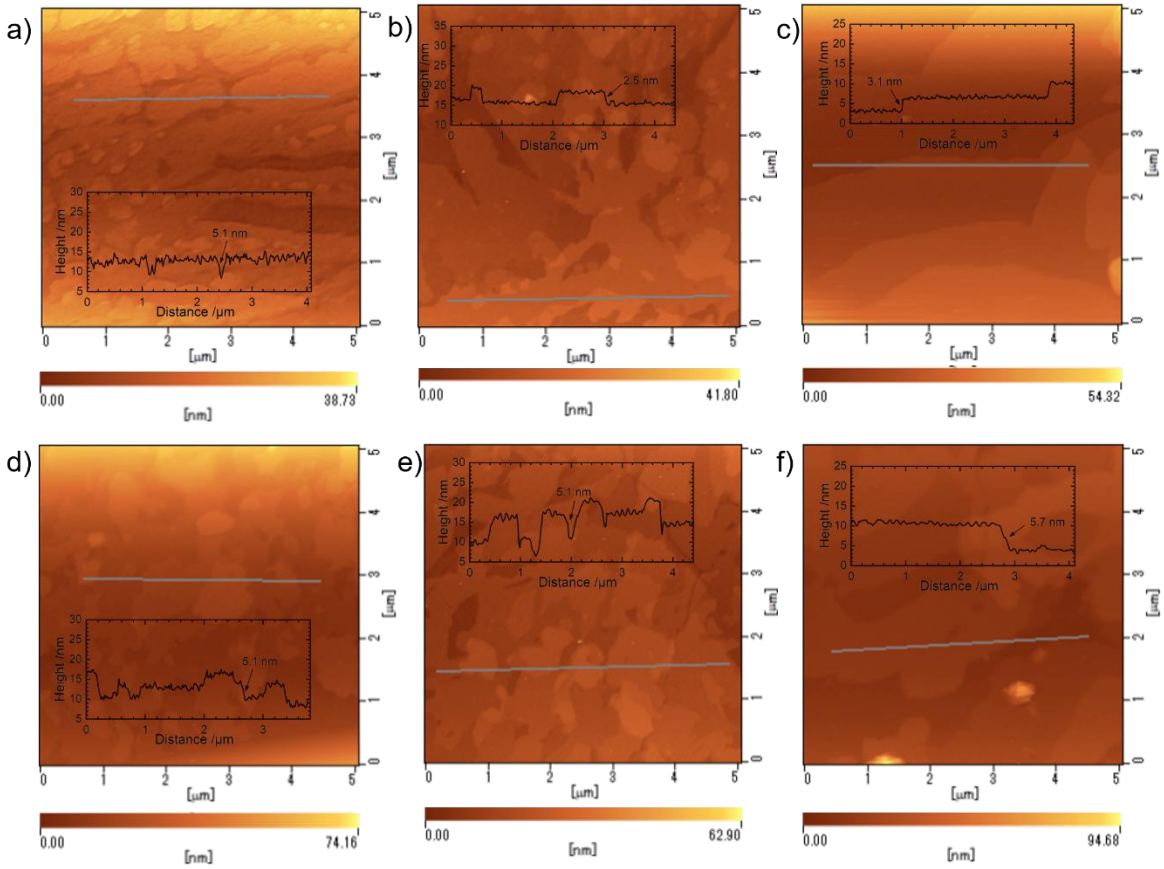

Figure S11: Atomic force microscopy images of polycrystalline thin films fabricated by spin-coating a 0.5 wt-% solution in *p*-xylene at 60 °C. Insets show cross-sectional profiles.: a),d) **12O-Az-T** as coated and annealed, b),e) **12O-Az-iT** as coated and annealed and c,f) **12O-Az-BT** as coated an annealed

9. References

1 F. Schulz, P. Ehni, B. Wank, A. Bauer, W. Frey and S. Laschat, Alkoxy-bromo-azulenes displaying ambient temperature smectic E-phases, *Liq. Cryst.*, 2021, **48**, 832–843.

2 J. J. Molloy, R. P. Law, J. W. B. Fyfe, C. P. Seath, D. J. Hirst and A. J. B. Watson, A modular synthesis of functionalised phenols enabled by controlled boron speciation, *Org. Biomol. Chem.*, 2015, **13**, 3093–3102.

3 N. Godbert, A. Crispini, M. Ghedini, M. Carini, F. Chiaravalloti and A. Ferrise, LCDiXRay: a user-friendly program for powder diffraction indexing of columnar liquid crystals, *J. Appl. Crystallogr.*, 2014, **47**, 668–679.

4 O. Treutler and R. Ahlrichs, Efficient molecular numerical integration schemes, *J. Chem. Phys.*, 1995, **102**, 346–354.

5 K. Eichkorn, O. Treutler, H. Öhm, M. Häser and R. Ahlrichs, Auxiliary basis sets to approximate Coulomb potentials, *Chem. Phys. Lett.*, 1995, **240**, 283–290.

6 M. V. Arnim and R. Ahlrichs, Performance of parallel TURBOMOLE for density functional calculations, *J. Comput. Chem.*, 1998, **19**, 1746–1757.

7 M. Sierka, A. Hogekamp and R. Ahlrichs, Fast evaluation of the Coulomb potential for electron densities using multipole accelerated resolution of identity approximation, *J. Chem. Phys.*, 2003, **118**, 9136–9148.

8 S. Grimme, J. Antony, S. Ehrlich and H. Krieg, A consistent and accurate ab initio parametrization of density functional dispersion correction (DFT-D) for the 94 elements H-Pu, *J. Chem. Phys.*, 2010, **132**, 154104.

9 S. Grimme, S. Ehrlich and L. Goerigk, Effect of the damping function in dispersion corrected density functional theory, *J. Comput. Chem.*, 2011, **32**, 1456–1465.

10 K. Eichkorn, O. Treutler, H. Öhm, M. Häser and R. Ahlrichs, Auxiliary basis sets to approximate Coulomb potentials (Chem. Phys. Letters 240 (1995) 283-290), *Chem. Phys. Lett.*, 1995, **242**, 652–660.

11 K. Eichkorn, F. Weigend, O. Treutler and R. Ahlrichs, Auxiliary basis sets for main row atoms and transition metals and their use to approximate Coulomb potentials, *Theor. Chem. Acc.*, 1997, **97**, 119–124.

12 F. Furche, R. Ahlrichs, C. Hättig, W. Klopper, M. Sierka and F. Weigend, Turbomole, *WIREs Comput. Mol. Sci.*, 2014, **4**, 91–100.

13 TURBOMOLE V7.1 2016, a development of University of Karlsruhe and Forschungszentrum Karlsruhe GmbH, 1989-2007, TURBOMOLE GmbH, since 2007; available from http://www.turbomole.com.

10. ^{1}H and ^{13}C NMR Spectra

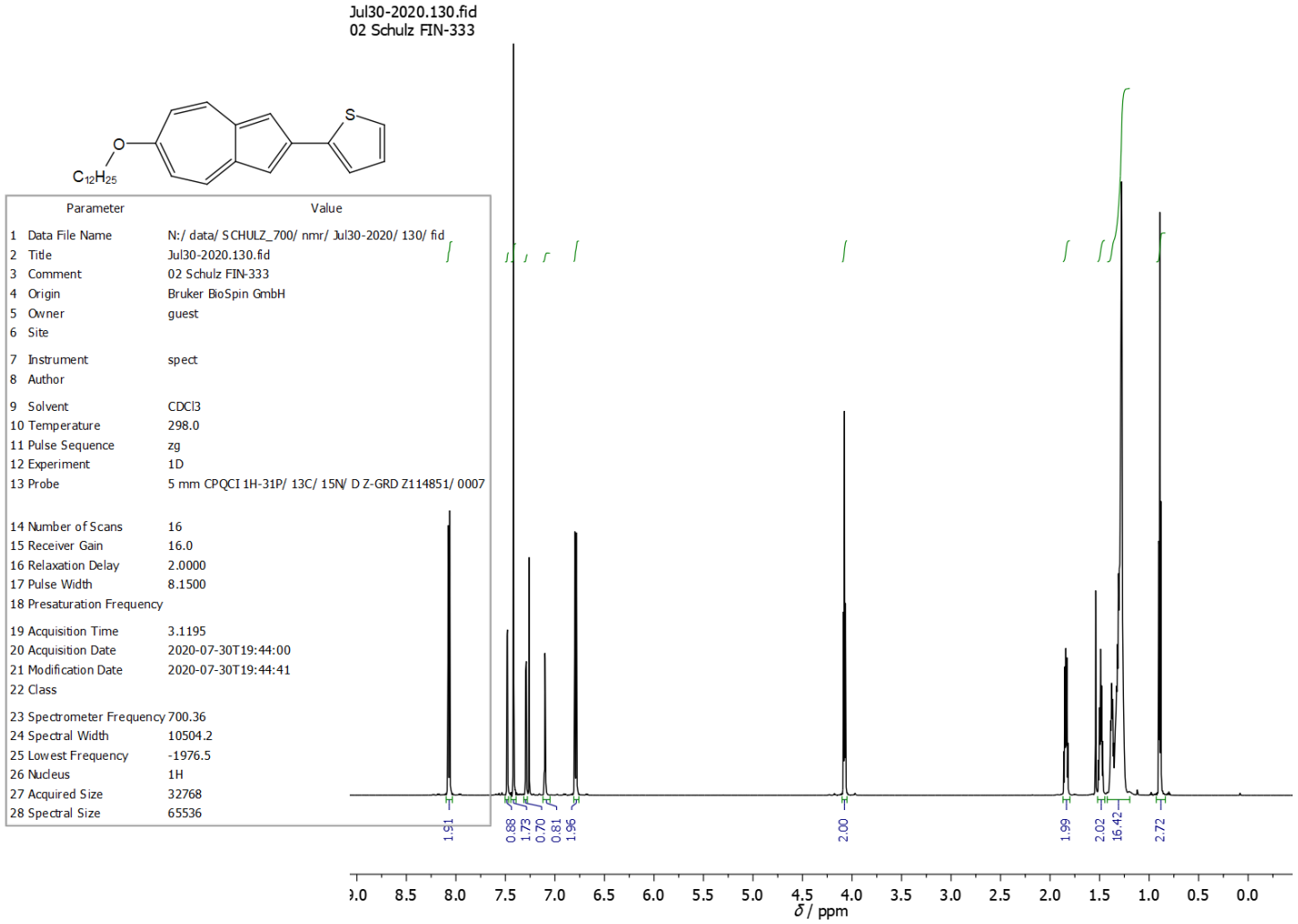

Figure S12: ^{1}H-NMR spectrum of **12O-Az-T**.

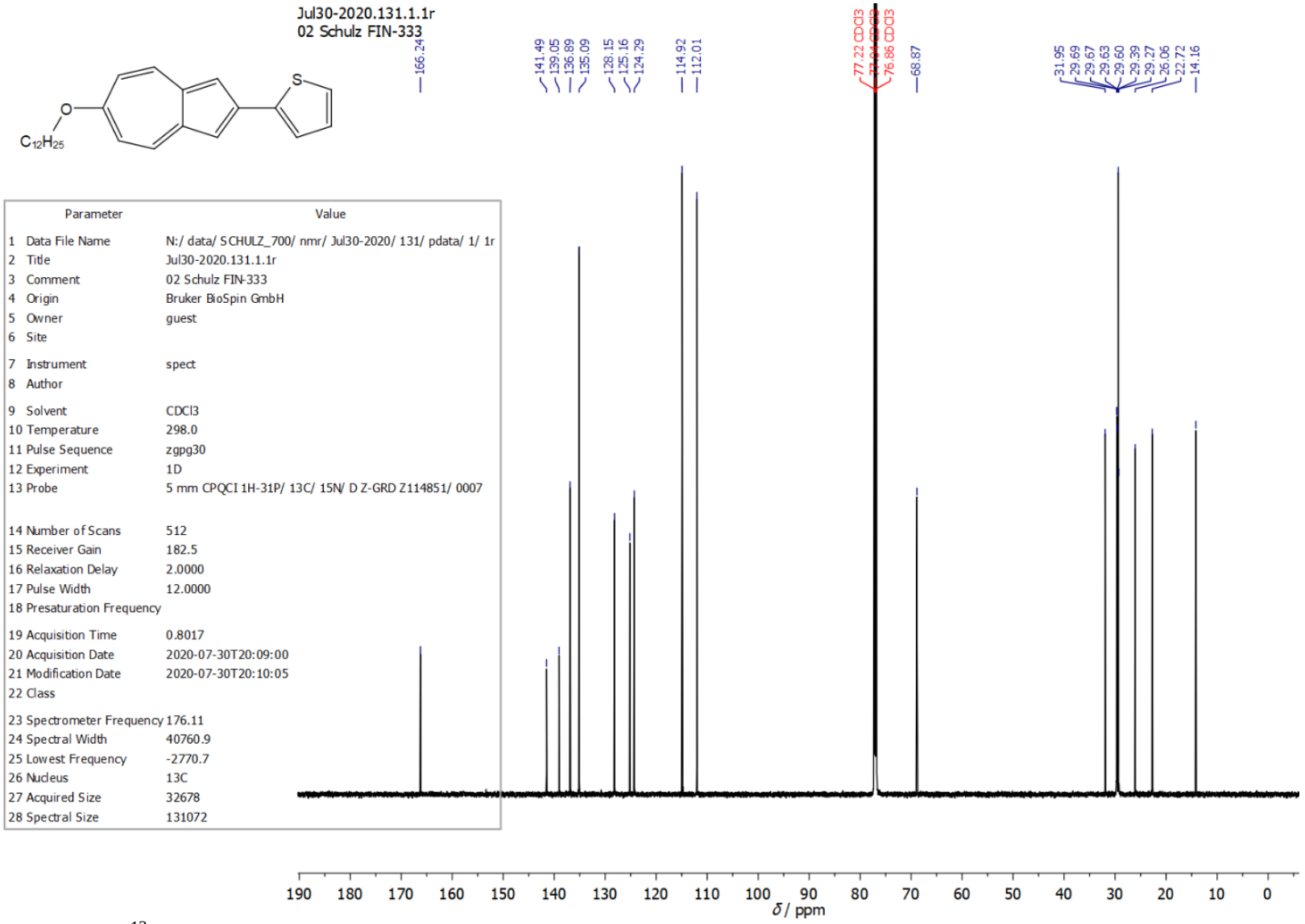

Figure S13: ^{13}C-NMR spectrum of **12O-Az-T**.

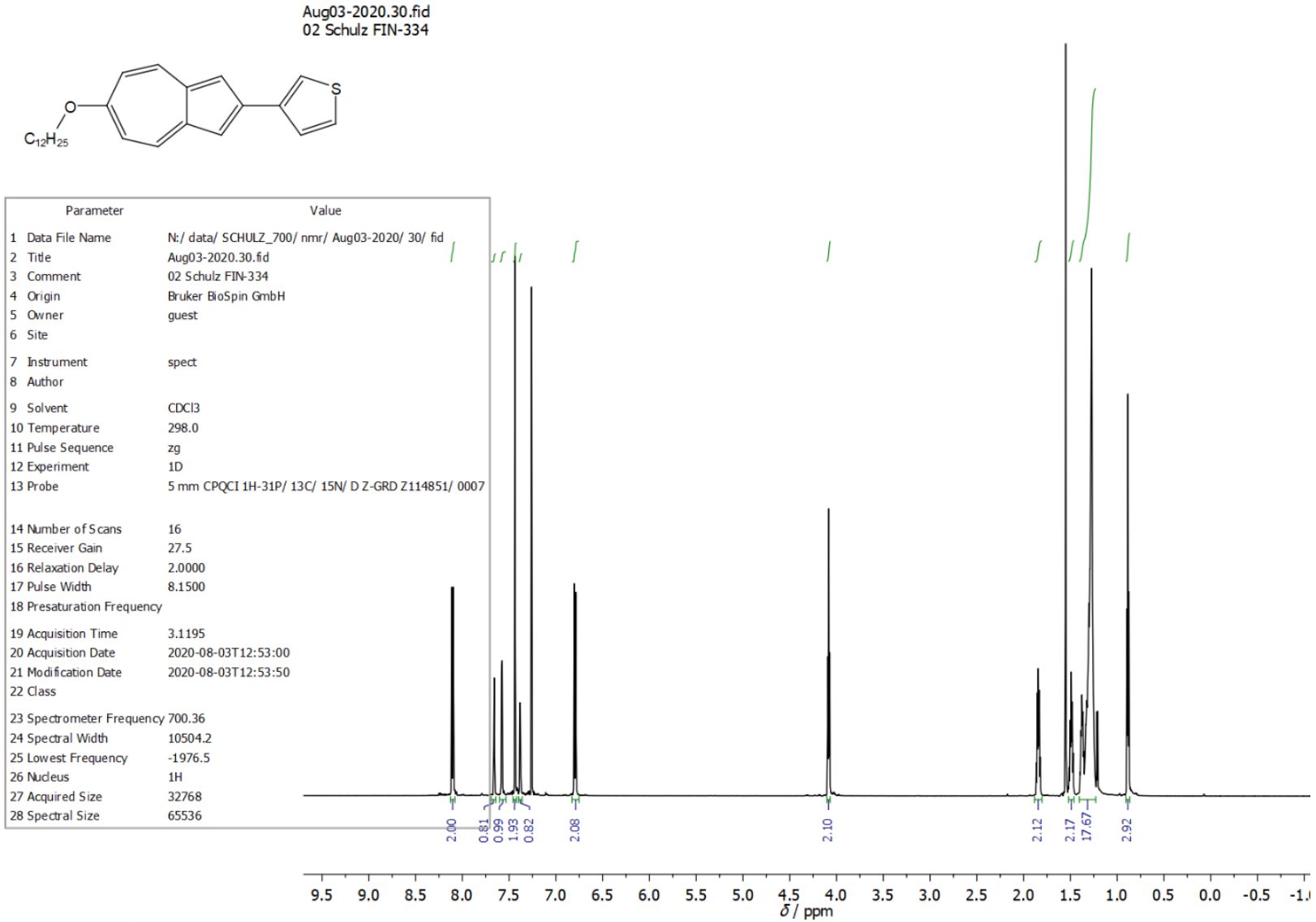

Figure S14: ^{1}H-NMR spectrum of **12O-Az-iT**.

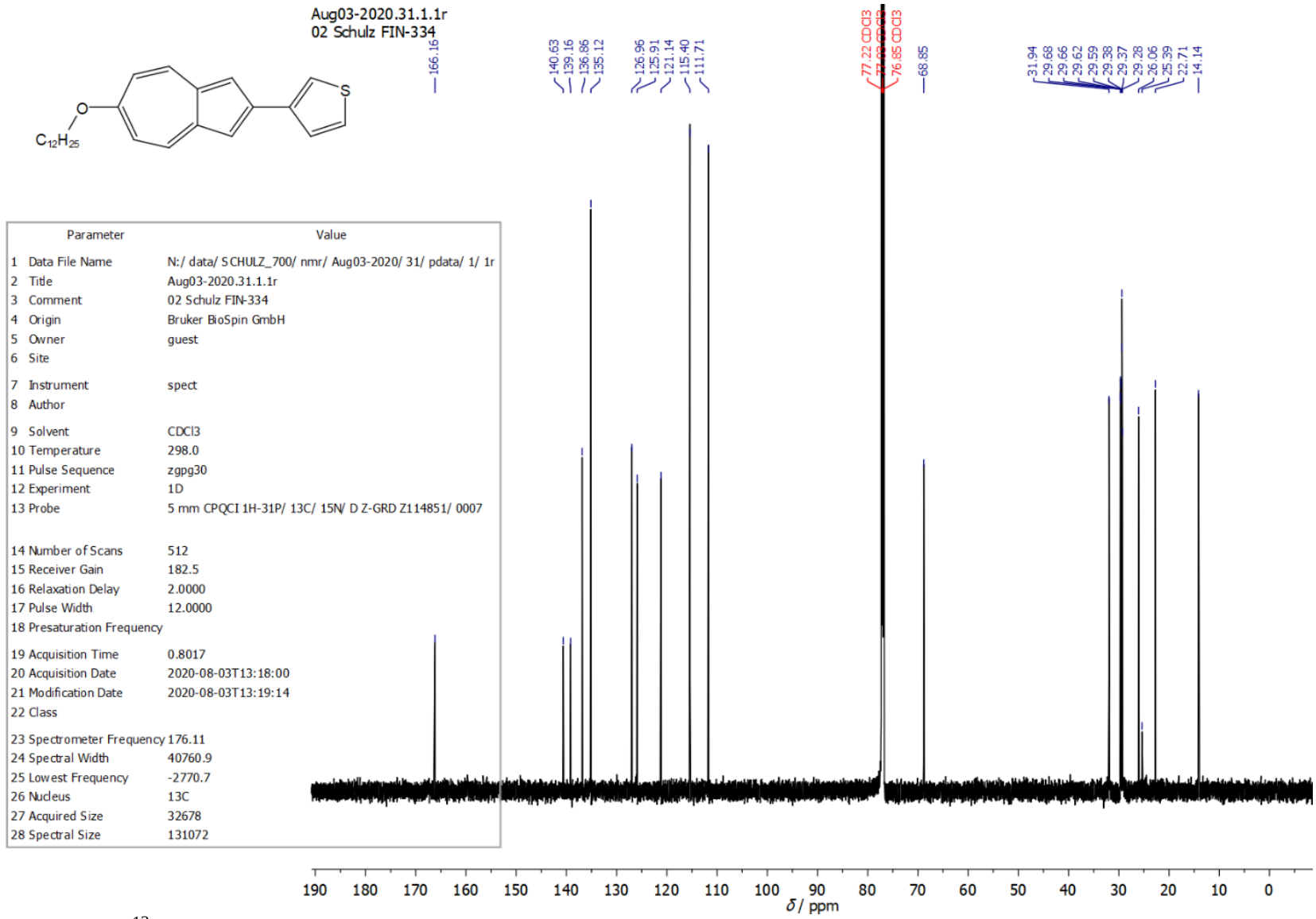

Figure S15: ^{13}C-NMR spectrum of **12O-Az-iT**.

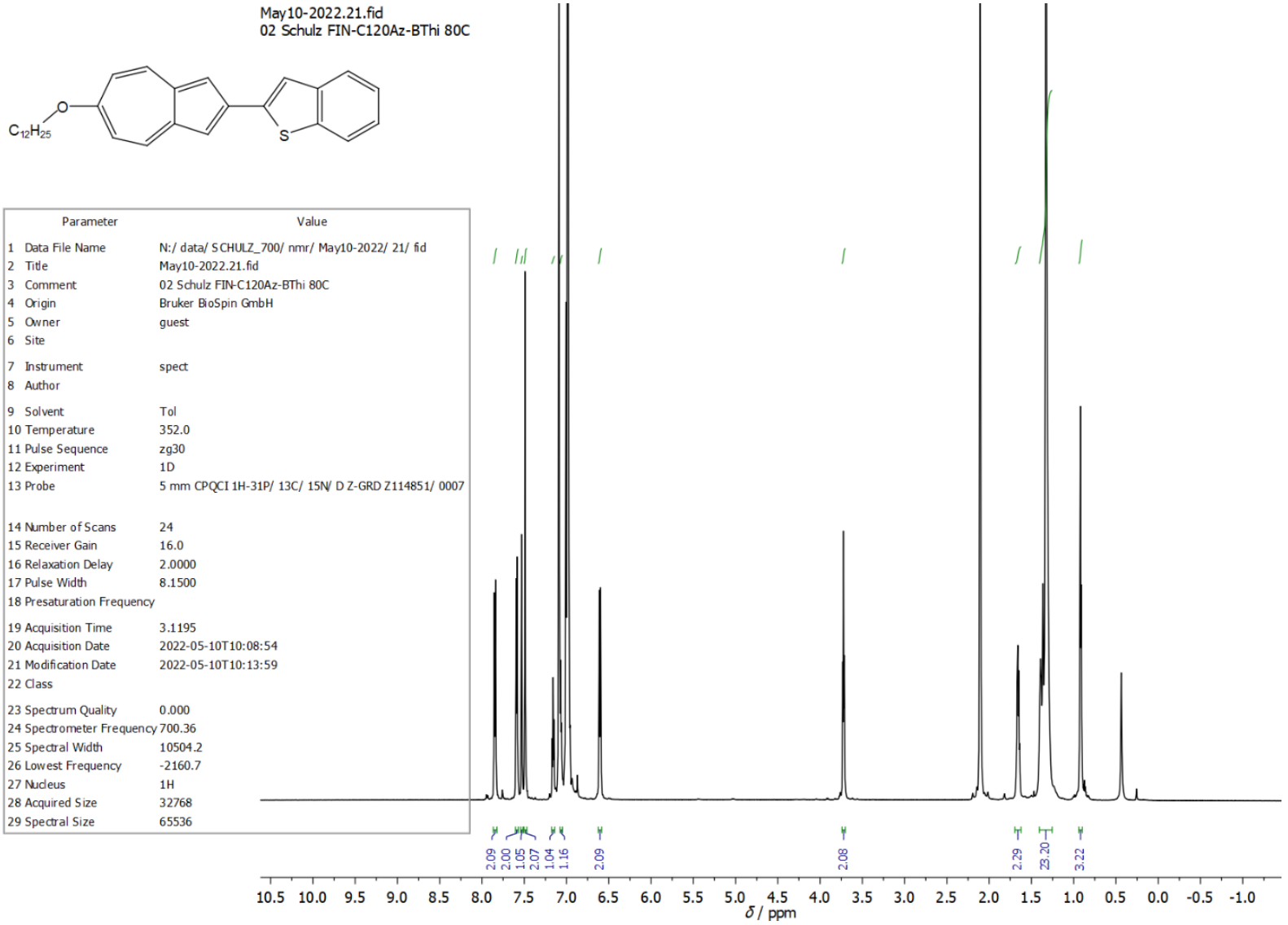

Figure S16: ^{1}H-NMR spectrum of **12O-Az-BT** at 80°C.

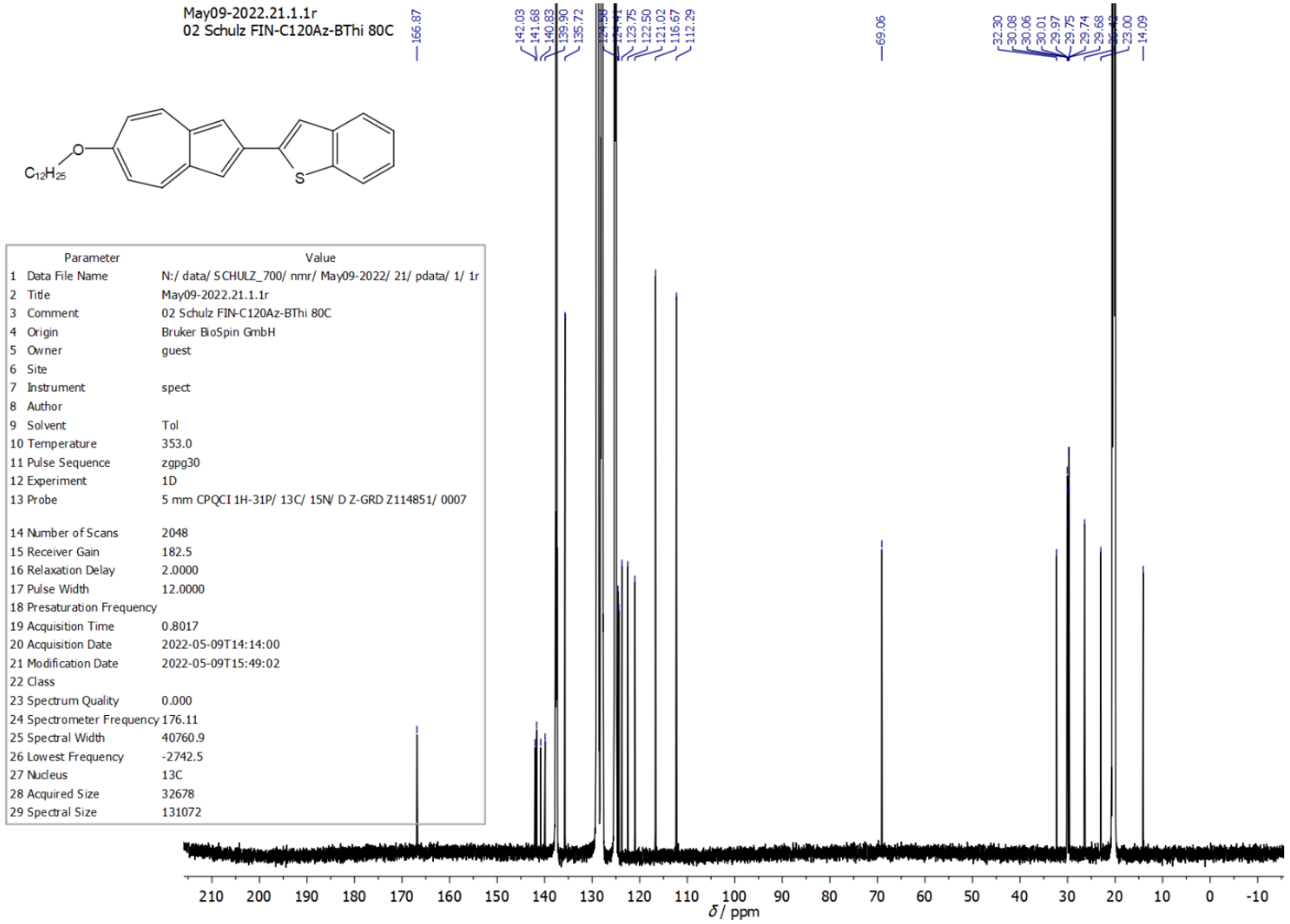

Figure S17: ^{13}C-NMR spectrum of **12O-Az-BT** at 80 °C.